Shape transitions in strained Cu islands on Ni(100): kinetics versus energetics

Yunsic Shim and Jacques G. Amar
Department of Physics & Astronomy
University of Toledo, Toledo, Ohio 43606, USA
(Dated: October 28, 2011)

We examine the ramified islands observed in submonolayer Cu/Ni(100) growth. Our results indicate that the strain-energy contribution to the dependence of island-energy on shape is surprisingly weak. In contrast, our accelerated dynamics simulations indicate that unexpected concerted popout processes occurring at step edges may be responsible. Kinetic Monte Carlo (KMC) simulations which include these processes produce island shapes which are very similar to those observed in experiment. These results suggest that the shape transition is of kinetic origin but is strongly mediated by strain.

PACS numbers: 68.35.Gy, 81.15.Aa, 68.55.-a

The morphological evolution of strained islands during heteropitaxial growth has recently been a topic of extensive experimental [1–10] and theoretical [11–13] studies in part due to its fundamental interest, but also because of possible applications to the formation of self-assembled nanostructures. Based on the results of continuum elasticity theory, it has been shown [11, 12], that in equilibrium the competition between the line-tension (which favors a compact shape) and strain-energy may lead to a spontaneous shape transition from compact to elongated islands above a critical island-size [3, 6, 10]. Recently, it has also been shown [14] that metastability may lead to an island-shape which reflects a local energy minimum which is not the equilibrium island-shape.

While much of the recent work has focused on the morphological evolution and stability of islands on semiconductor surfaces, it is also of interest to consider the case of growth on a metal substrate. Of particular interest is the case of Cu/Ni(100) growth [4, 5] for which a transition, with increasing island-size, from compact to ramified islands has been observed over a wide range of temperatures ($T = 250 - 345$ K). Since the temperature in the experiments was sufficiently high that rapid island-relaxation is expected, it was suggested [4, 5] that the transition may be explained by energetic arguments based on a competition between line-tension and strain-energy.

In this Letter, we present the results of energetics calculations as well as temperature-accelerated dynamics (TAD) [15] and kinetic Monte Carlo (KMC) simulations which indicate that the shape transition is not primarily determined by energetic effects, but is instead due to kinetic effects which are mediated by strain. In particular, by calculating the relevant line-tension and strain energies, and comparing with recent continuum elasticity predictions of Ref. 12 for the dependence of the critical island-width L_c on these quantities, we demonstrate that the equilibrium critical island-width is at least four orders of magnitude larger than the experimentally estimated critical value $L_c \simeq 22$. In contrast, our TAD simulations indicate that unexpected concerted motions occurring at step edges may be responsible. The energy barriers for these concerted motions are significantly lower than for Cu/Cu(100) and Ni/Ni(100), decrease with increasing island size, and appear to saturate for islands larger than 300 - 400 atoms. By including these strain-induced kinetic processes in our KMC simulations of island-growth, we find that both the temperature-dependence and the coverage-dependence of the island morphology may be explained.

For an $L \times L$ square island (where L is in units of the nearest-neighbor distance b) with isotropic line-tension γ, the results of Ref. 12 imply that the critical island-width L_c for a transition from square to anisotropic islands is given by,

$$L_c = a_0 \exp\left[\frac{\alpha + 2}{2(1-\nu)} + 1.30\right], \qquad (1)$$

where a_0 is a short-distance cutoff of the order of the lattice constant, $\alpha = \gamma/E_u$ is the ratio of the island line-tension to the unit strain energy $E_u = \frac{1+\nu}{2\pi\mu}F^2$, F is the force density along the periphery of the island, and μ and ν are the Young's modulus and Poisson ratio of the substrate. Accordingly, to estimate the equilibrium value of L_c we have first calculated the zero-temperature line-tension $\gamma_{110}(0)$ for closed-steps, by determining the size-dependence of the island-energy (determined by subtracting the energy of the bare substrate from the energy of the system with an island on top) for $L \times L$ square Cu/Ni(100) islands, as shown schematically in Fig. 1 [16]. Our calculations were carried out using an embedded-atom method (EAM) potential [17] (hereinafter called MVB). In particular, we have calculated the island energy $E(L)$ on a "native" Ni substrate corresponding to 2.6% strain, as well as the island energy $E_m(L)$ for a "matched" Ni(100) substrate which has been expanded so that there is no strain between the Cu and the Ni. For the matched substrate we expect that the size-dependent island-energy should have the form $E_m(L) = E_m(\infty) + (4\gamma_{110}\ b)/L$ plus corner-

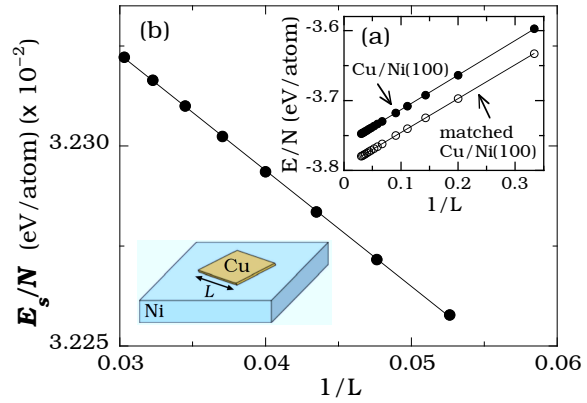

FIG. 1: (a) Island energy per atom E/N for square islands on "native" and matched substrates as function of island-size L for $L = 19$ to 33. (b) Strain-energy per atom E_s/N as function of island-size L. Picture shows Cu/Ni(100) island, with substrate consisting of 3 moving and 3 fixed (bottom) layers and lateral size $L_{sub} = 100$ in units of $b_0 = a/2$ where a is the lattice constant.

corrections and indeed we find for the (per atom) island-energy, $E_m(L)/N = -3.794\ eV + 0.492\ eV/L$ (where $N = L^2$) which implies $\gamma_{110} \simeq 0.048$ eV/Å, while for the "native substrate" we find $E(L)/N = -3.762\ eV + 0.489\ eV/L$. Subtracting, leads to the strain-energy per atom, $E_s(L)/N = 0.0324\ eV - 0.00289\ eV/L$. Surprisingly, while the asymptotic value of the strain energy $E_s(\infty)/N \simeq 0.032$ eV is in reasonable agreement with continuum expressions [18], the finite-size correction is significantly smaller than the continuum prediction [12].

As a check on our results, we have also calculated γ_{110} by making the assumption that - ignoring the strain contribution - the energy of a Cu/Ni(100) island may be approximated as a sum of nearest-neighbor and next-nearest-neighbor interactions of strength ϵ_1 and ϵ_2 respectively [19]. As shown in Table I, we have carried out both density-functional theory (DFT) calculations using the Vienna Ab-initio Simulation Package (VASP)[20], as well as calculations using several different EAM potentials including the MVB potential, an "AFW" potential developed by Adams, Foiles, and Wolfer [21], and a potential developed by Zhou et al [22]. The line-tensions for open and closed steps may then be calculated using the expressions [19], $\gamma_{100} = \frac{\epsilon_1+\epsilon_2}{\sqrt{2}}$ and $\gamma_{110} = \frac{\epsilon_1}{2} + \epsilon_2$. As can be seen, there is good agreement between the MVB result calculated using this method and our previous calculation, while the DFT value is also in good agreement with this value. In addition, we have calculated the unit strain energy E_u for a Cu/Ni(100) island using the method described in Ref. 9, which involves calculating the substrate and film stresses σ^s_{xx} and σ^f_{xx} to obtain the force density $F_x = \sigma^f_{xx} - \sigma^s_{xx}$.

Table I shows a summary of our results for γ_{110}, E_u, and the corresponding critical island-width L_c calculated

TABLE I: Comparison of DFT results for line tension, unit strain energy (E_u) and critical island width (L_c) with results obtained using three different EAM potentials. For the EAM calculations a substrate size $L_{sub} = 40$ and a slab of 7 moving and 3 fixed layers were used to obtain σ^s_{xx} and σ^f_{xx}.

	EAM			
	MVB [17]	AFW [21]	Zhou [22]	DFT
γ_{110} (eV/Å)	0.049	0.065	0.085	0.044
γ_{100} (eV/Å)	0.062	0.084	0.095	0.059
σ^s_{xx} (eV/Å^2)	0.146	0.083	0.103	0.175
σ^f_{xx} (eV/Å^2)	-0.020	0.045	0.030	0.041
F_x (eV/Å^2)	-0.148	-0.038	-0.073	-0.134
E_u (eV/Å)	3.7×10^{-3}	2.4×10^{-4}	8.9×10^{-4}	3.0×10^{-3}
L_c	2.6×10^{5}	1.5×10^{86}	1.9×10^{31}	6.5×10^{5}

using Eq. 1 with $a_0 = b$. As can be seen, while there are some variations in the unit strain-energy E_u and line-tension γ, in all cases the calculated critical island-size L_c for the transition to anisotropic islands is at least four orders of magnitude larger than the typical branch width ($w \simeq 22$ atoms) observed in experiments. We expect that due to thermal fluctuations the perimeter free-energy $\gamma(T)$ is likely to be reduced at experimental temperatures, but by calculating the free-energy based on our estimated values for ϵ_1 and ϵ_2 (see Ref. 19) we find that this effect is relatively small ($6 - 14$ % decrease at 345 K) and so the calculated value of the critical island-width L_c is not significantly reduced by this effect. As a result, our energetic calculations strongly suggest that the experimentally observed ramified shapes cannot be explained by continuum elasticity theory but instead are of kinetic origin.

In order to further investigate this possibility we have carried out TAD annealing simulations at 300 K using the MVB EAM potential for an initial configuration consisting of an 11×11 square Cu island (as shown in Fig. 1) along with two edge-atoms at one corner of the island. During the TAD simulation (which lasted 2 ms) a variety of island-rearrangement processes were observed including several unexpected in-plane 'popout' processes which involve two or more atoms moving together along $\langle 110 \rangle$ directions. Fig. 2(a) shows a schematic diagram of some of these processes along with the corresponding forward and reverse activation barriers. As can be seen, the presence of kink sites significantly decreases the barrier for a popout process. Furthermore, if the reverse barrier is sufficiently high, then the vacancy created may migrate away and be eventually emitted at an island edge. Along with one-atom popout these multi-atom popout processes tend to destabilize step-edges, converting closed steps to open steps and vice-versa, thus creating a competition between open and closed steps. Also, as shown in Fig. 2(b) the corresponding activation energies decrease with increasing island-width L until a saturation width which is close to the experimentally ob-

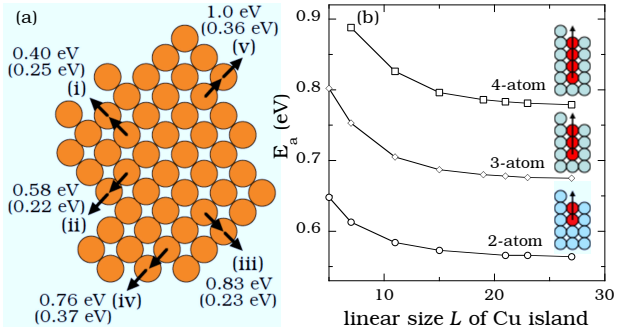

FIG. 2: (a) Schematic diagram of five in-plane popout processes with corresponding barriers used in KMC simulations (numbers in parentheses are energy barriers for reverse processes). (b) Energy barriers E_a as function of the size of a strained square Cu island and the number of atoms involved in the process. Here the substrate size $L_{sub} = 60$ with 3 moving and 3 fixed layers.

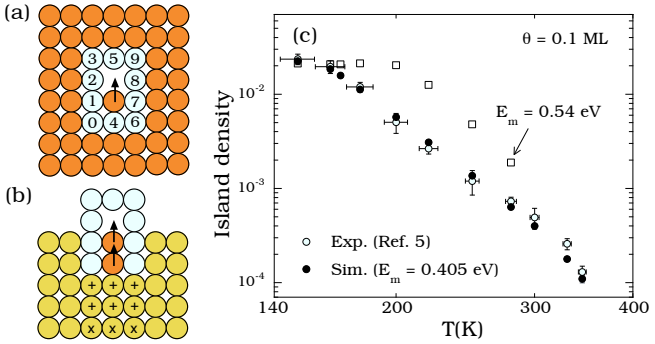

FIG. 3: Schematic diagrams showing neighboring atoms (open circles) corresponding to different configurations considered in barrier calculations for (a) single atom diffusion and (b) two-atom popout. Orange (yellow) atoms indicate 'embedding region'. (c) Comparison of KMC and experimental results for the temperature-dependence of the island density [5] (deposition flux $F = 0.0015$ ML/s).

served selected arm-width $L_{exp} \simeq 22$. We have also verified that if the strain is artificially increased by compressing the Ni substrate then the barriers are further reduced, while in the absence of strain or in the presence of tensile-strain they are significantly higher.

To further understand the effects of strain on the island morphology, we have carried out KMC simulations of Cu/Ni(100) island growth in which these processes are incorporated (a total of 35 different multi-atom popout mechanisms were included, see Fig. 3(b)) with barriers calculated using the MVB EAM potential [23]. As shown in Table II, our KMC model also includes key barriers for edge-zipping [24], single-bond edge-diffusion, dimer detachment, and vacancy diffusion which were obtained from DFT calculations [25], although a somewhat reduced value of the monomer diffusion barrier (close to the experimentally deduced value 0.37 ± 0.03 eV [5]) was used in order to match the experimental island density over the temperature range $T = 140 - 350$ K (see Fig. 3(c)). Corner detachment with a barrier of 0.56 eV [4] was also included.

In addition to these key barriers, a variety of additional forward and reverse barriers and prefactors for single-atom diffusion were calculated as a function of the 1024 local configurations shown in Fig. 3(a). Since the AFW EAM barriers in Table II are in good agreement with the DFT results, for all of these single-atom processes we have used the AFW EAM potential with the barriers slightly modified to be consistent with DFT results. Also, in order to take into account longer-range interactions due to strain and/or 'pinning' effects [24], in all cases except for the barriers shown in Table II, we have assumed that the diffusing atoms were embedded in the middle (or edge) of an 11×11 island as shown in Fig. 3.

Fig. 4 shows our KMC simulation results for the island morphology at $T = 250$ K with a deposition flux $F = 1.5 \times 10^{-3}$ ML/s as in the experiment. In particular, as shown in Fig. 4(a) - and in good agreement with the corresponding experimental pictures in Ref. 4 - at a coverage of 0.09 monolayers (ML) the islands are typically compact but with a mixture of closed [110] and open [100] step-edges, which leads to "obtuse" corners with an angle of 135^o as well as "acute" corners with an angle of 45^o degrees. As these islands grow, the competition between open and closed steps leads to somewhat elongated structures whose further coalescence is enhanced by popout events thus leading to the ramified islands shown in Fig. 4(b), which are similar to the corresponding STM pictures in Ref. 4 and Ref. 5. In contrast, if all multiatom popout processes are suppressed then only open steps are observed and coalescence is significantly reduced as shown in Fig. 4(c). As a result the islands tend to remain compact even at high coverage [26].

Also shown in Fig. 4 is the island morphology obtained from our simulations at $T = 300$ K at coverage $\theta = 0.3$ ML. In good agreement with the corresponding experimental pictures shown in Ref. [5], the islands are reasonably compact but exhibit a competition between open and closed steps. The fact that the experimental islands

TABLE II: Comparison of energy barriers (eV) for diffusion processes obtained from three EAM potentials and DFT calculations for Cu/Ni(100). In the EAM calculations, a substrate with lateral size $L_{sub} = 24$ and 3 moving and 3 fixed layers was used. The size in DFT indicates the supercell size (in units of b) used in the calculation.

Diffusion mechanism	E_a (eV)				
	MVB	AFW	Zhou	DFT (size)	Model
monomer	0.50	0.54	0.51	0.54 (4×4)	0.41
edge-diffusion	0.33	0.33	0.33	0.35 (4×6)	0.35
edge-zipping	0.15	0.08	0.08	0.17 (4×5)	0.20
dimer detachment	0.70	0.80	0.78	0.78 (4×5)	0.80
single vacancy	0.25	0.33	0.24	0.33 (4×4)	0.33

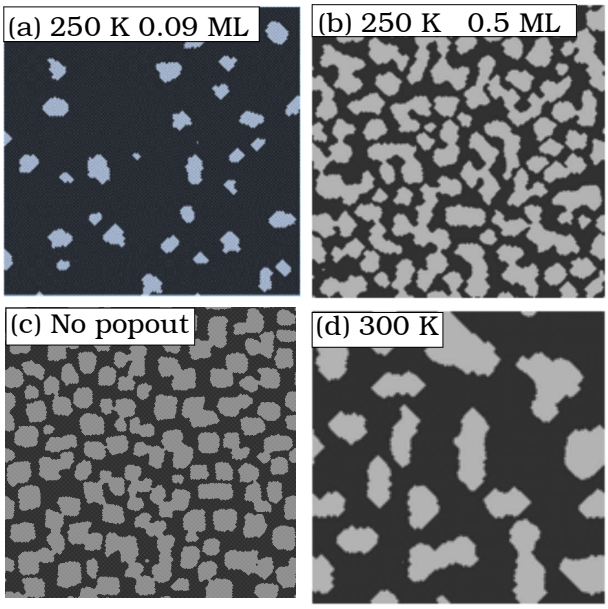

FIG. 4: Surface morphologies (200×200 portion) obtained from KMC simulations with $L_{sub} = 400$ and $F = 1.5 \times 10^{-3}$ ML/s. (a) $\theta = 0.09$ ML at 250 K (b) $\theta = 0.5$ ML at 250 K (c) same as (b) but without multiatom popout processes (d) $\theta = 0.3$ ML at 300 K.

at this coverage and temperature are still not ramified, even though they are significantly larger than obtained experimentally at 250 K and 0.5 ML, is also consistent with our energetics calculations which indicate that the critical island-width for the transition from compact to ramified islands is orders of magnitude larger than the experimental island sizes. This is further supported by the experimental observation [5] that annealing at 500 K leads to islands which are even more compact.

We have also carried out KMC simulations using our model at a higher temperature (345 K) at which the transition from compact to ramified islands is found to occur experimentally at relatively low coverage (0.15 ML). In this case, while there is reasonable agreement between our simulations and the experimental morphology at $\theta = 0.09$ ML, at higher coverage our KMC simulations lead to elongated islands rather than the ramified islands observed in experiment. We speculate that this may be due to the existence of higher-barrier processes which "turn-on" at higher temperature but which are not included in our model.

In conclusion, both our KMC simulations and energetics calculations indicate that the shape transition from compact to ramified islands in Cu/Ni(100) growth may be explained by kinetic processes rather than energetics. In particular, the competing mechanisms of edge smoothing and roughening induced by strain, along with the effects of coalescence, can explain the ramified island shapes observed up to 300 K. For higher temperatures one may have to explicitly take into account the complex interplay between the size dependence of activated processes and strain to explain the experimental island shape.

This work was supported by NSF grant DMR-0907399. We would also like to acknowledge a grant of computer time from the Ohio Supercomputer Center.

[1] Y.-W. Mo *et al.*, Phys. Rev. Lett. **65**, 1020 (1990).
[2] A. Brodde *et al.*, J. Vac. Sci. Technol. B **9**, 920 (1991).
[3] S. H. Brongersma *et al.*, Phys. Rev. Lett. **80**, 3795 (1998).
[4] B. Müller *et al.*, Phys. Rev. Lett. **80**, 2642 (1998).
[5] B. Müller *et al.*, Surf. Rev. Lett. **5**, 769 (1998); *ibid.* **8**, 169 (2001).
[6] W. Ma *et al.*, Appl. Phys. Lett. **79**, 4219 (2001).
[7] V. Fournée *et al*, Phys. Rev. B **67**, 155401 (2003).
[8] I. Goldfarb *et al.*, Phys. Rev. Lett. **97**, 206101 (2006).
[9] Y. Li *et al.*, Phys. Rev. Lett. **103**, 076102 (2009); G.-H. Lu and F. Liu, *ibid.* **94**, 176103 (2005).
[10] M. S. J. Marshall and M. R. Castell, Phys. Rev. Lett. **102**, 146102 (2009).
[11] J. Tersoff and R.M. Tromp, Phys. Rev. Lett. **70**, 2782 (1993).
[12] A. Li, F. Liu, and M.G. Lagally, Phys. Rev. Lett. **85**, 1922 (2000).
[13] H. J. Zandvliet and R. van Gastel, Phys. Rev. Lett. **99**, 136103 (2007).
[14] N.V. Medhekar et al, Phys. Rev. Lett. **99**, 156102 (2007).
[15] M. R. Sørensen and A. F. Voter, J. Chem. Phys. **112**, 9599 (2000).
[16] We have verified that for the island-sizes studied the island-energy is independent of substrate-size for larger substrate-sizes, while a careful analysis of the substrate thickness dependence indicates that this leads to only a 1-2 percent deviation from the asymptotic result corresponding to an infinitely thick substrate.
[17] Y. Mishin et al, Phys. Rev. B **63**, 224106 (2001); A.F. Voter and S.P. Chen, Mater. Res. Soc. Symp. Proc. 82 175 (1987); For the cross potential, see G. Bonny *et al.*, Phil. Mag. **89**, 3531 (2009).
[18] A. Pimpinelli and J. Villain, *Physics of Crystal Growth* (Cambridge, London) 1999.
[19] R. Van Moere *et al.*, Phys. Rev. B **67**, 193407 (2003).
[20] G. Kresse and J. Hafner, Phys. Rev. B **47**, 558 (1993); *ibid.* **49**, 14251 (1994).
[21] J. B. Adams, S. M. Foiles, and W. G. Wolfer, J. Mater. Res. **4**, 102 (1989). For the cross potential $\phi_{\mathrm{Cu-Ni}}$ we used the form given in S. M. Foiles, M. I. Baskes, and M. S. Daw, Phys. Rev. B **33**, 7983 (1986).
[22] X. W. Zhou *et al.*, Phys. Rev B **69**, 144113 (2004).
[23] In our KMC simulations, two-atom (three-atom) popouts were only allowed if all sites marked '+' (as well as sites marked 'x') in Fig. 3(b) were occupied.
[24] Y. Shim and J. G. Amar, Phys. Rev. B **83**, 245419 (2011).
[25] In Table II, edge zipping corresponds to the case that only sites (2) and (8) in Fig. 3(a) are occupied and dimer detachment corresponds to the case that only site (4) is occupied.
[26] If single-atom popout is also suppressed, then closed steps dominate and again the islands remain compact.